PROCEEDINGS OF SPIE

SPIEDigitalLibrary.org/conference-proceedings-of-spie

The Galaxy Evolution Probe: a concept for a mid and far-infrared space observatory

Jason Glenn, C. Matt Bradford, Rashied Amini, Bradley Moore, Andrew Benson, et al.

Jason Glenn, C. Matt Bradford, Rashied Amini, Bradley Moore, Andrew Benson, Lee Armus, Katherine Alatalo, Jeremy Darling, Peter Day, Jeanette Domber, Duncan Farrah, Adalyn Fyhrie, Brandon Hensley, Sarah Lipscy, David Redding, Michael Rogers, Mark Shannon, John Steeves, Carole Tucker, Gordon Wu, Jonas Zmuidzinas, "The Galaxy Evolution Probe: a concept for a mid and far-infrared space observatory," Proc. SPIE 10698, Space Telescopes and Instrumentation 2018: Optical, Infrared, and Millimeter Wave, 106980L (24 July 2018); doi: 10.1117/12.2314076

SPIE.

Event: SPIE Astronomical Telescopes + Instrumentation, 2018, Austin, Texas, United States

The Galaxy Evolution Probe: A concept for a mid and far-infrared space observatory

Jason Glenn*[a], C. Matt Bradford[b], Rashied Amini[b], Bradley Moore[b], Andrew Benson[c], Lee Armus[d], Katherine Alatalo[e], Jeremy Darling[a], Peter Day[b], Jeanette Domber[f], Duncan Farrah[g], Adalyn Fyhrie[a], Brandon Hensley[b], Sarah Lipscy[f], David Redding[b], Michael Rodgers[b,h], Mark Shannon[f], John Steeves[b], Carole Tucker[i], Gordon Wu[f], Jonas Zmuidzinas[b,j]

[a]Center for Astrophysics and Space Astronomy, University of Colorado, 389-UCB, Boulder, CO 80309; [b]JPL, 4800 Oak Grove Drive, Pasadena, CA 91109; [c]Observatories of the Carnegie Institution for Science, 813 Santa Barbara Street, Pasadena, CA 91101; [d]Infrared Processing and Analysis Center, 1200 East California Blvd., MC 314-6, Pasadena, CA 91125; [e]Space Telescope Science Institute, 3700 San Martin Drive, Baltimore, MD 21218; [f]Ball Aerospace, 1600 Commerce St. Boulder, CO 80301; [g]Department of Physics MC 0435, 850 West Campus Drive, Virginia Tech, Blacksburg, VA 24061; [h]Synopsys, Inc., 199 South Los Robles Ave., Suite 400, Pasadena, CA 91101; [i]School of Physics and Astronomy, Cardiff University, Cardiff, CF24, UK; [j]Dept. of Physics, Mathematics, and Astronomy, Caltech, 1200 E. California Blvd., Pasadena, CA 91125

ABSTRACT

The Galaxy Evolution Probe (GEP) is a concept for a mid and far-infrared space observatory designed to survey sky for star-forming galaxies from redshifts of $z = 0$ to beyond $z = 4$. Furthering our knowledge of galaxy formation requires uniform surveys of star-forming galaxies over a large range of redshifts and environments to accurately describe star formation, supermassive black hole growth, and interactions between these processes in galaxies. The GEP design includes a 2 m diameter SiC telescope actively cooled to 4 K and two instruments: (1) An imager to detect star-forming galaxies and measure their redshifts photometrically using emission features of polycyclic aromatic hydrocarbons. It will cover wavelengths from 10 to 400 μm, with 23 spectral resolution $R = 8$ filter-defined bands from 10 to 95 μm and five $R = 3.5$ bands from 95 to 400 μm. (2) A 24 – 193 μm, $R = 200$ dispersive spectrometer for redshift confirmation, identification of active galactic nuclei, and interstellar astrophysics using atomic fine-structure lines. The GEP will observe from a Sun-Earth L2 orbit, with a design lifetime of four years, devoted first to galaxy surveys with the imager and second to follow-up spectroscopy. The focal planes of the imager and the spectrometer will utilize KIDs, with the spectrometer comprised of four slit-coupled diffraction gratings feeding the KIDs. Cooling for the telescope, optics, and KID amplifiers will be provided by solar-powered cryocoolers, with a multi-stage adiabatic demagnetization refrigerator providing 100 mK cooling for the KIDs.

Keywords: Galaxy Evolution Probe, space observatory, star-forming galaxies, mid infrared, far infrared, polycyclic aromatic hydrocarbons, kinetic inductance detectors

1. INTRODUCTION

NASA currently has no Astrophysics mission class intermediate between MIDEXs (capped at ~$250M, not including launch vehicles) and large Surveyor class missions. An intermediate class, NASA Astrophysics Probes – analogous to the successful New Frontiers NASA planetary missions, would enable more ambitious science than SMEXs and MIDEXs but with a higher cadence than Surveyors. A Probe class with a mission cadence of one or more per decade would greatly improve the ability of the astrophysics community to respond to new scientific discoveries, and with a $1B cost cap Probes would present a less risky and more nimble alternative than Surveyor class missions. It is also likely that Probes could serve as pathfinders for the Surveyor missions, as could be the case for the Galaxy Evolution Probe and the Origins Space Telescope. The Galaxy Evolution Probe (GEP) is a concept for a mid and far-infrared space observatory that will do large surveys of star-forming galaxies to provide essential new insights into star formation over cosmic time.

* Send correspondence to J. Glenn: E-mail: jason.glenn@colorado.edu

Space Telescopes and Instrumentation 2018: Optical, Infrared, and Millimeter Wave, edited by Makenzie Lystrup, Howard A. MacEwen, Giovanni G. Fazio, Proc. of SPIE Vol. 10698, 106980L
 · doi: 10.1117/12.2314076

1.1 The cosmic history of star formation

The last two and a half decades have witnessed major advances in our understanding of galaxy evolution. Observations across the electromagnetic spectrum, theoretical models, and numerical simulations have all contributed. Key aspects of star formation in galaxies have been revealed by infrared observations in particular. Infrared observations pierce the dusty environments in which stars form, they present techniques for measuring star formation rates without large extinction corrections, and they identify deeply obscured active galactic nuclei (AGN). The basic shape of the comoving star formation rate density in galaxies is now known:[1] it rose from a low rate in the first billion years after the Big Bang to a peak around $z \sim 1.5$ (when the Universe was about 4 billion years old), then declined very steeply, perhaps a factor of 30, to the present day. The reasons for this precipitous drop are not known, and mysterious because most of the baryons in the Universe had not been incorporated into stars by $z \sim 1.5$. It is possible that energetic feedback from AGN quenched star formation in high-mass galaxies, while supernovae and winds from hot stars helped to regulate star formation in low-mass galaxies. However, observational data are insufficient to support or reject this hypothesis. To address this, the GEP will deliver an unprecedented data set to measure the rates of star formation and the incidence of deeply obscured AGN in galaxies for a broad range of galaxy luminosities, in a broad range of environments (dark matter halo masses), and from redshifts ($z \sim 4$) prior to the peak in cosmic star formation history to the present day.

Given the large far-infrared/submillimeter data sets from, e.g., the *Herschel Space Observatory*, to make a significant leap in our understanding of galaxy evolution, new infrared galaxy surveys must measure the redshifts of the galaxies that they detect. GEP will do this using broad emission features of polycyclic aromatic hydrocarbons (PAHs), which arise from C-C and C-H bending and stretching modes. The mid and far-infrared spectra of galaxies are comprised of several main features: continuum emission in the far infrared and submillimeter from interstellar dust at temperatures of tens of Kelvin, continuum emission from warmer dust (in close proximity to stars or AGN) in the mid infrared, PAH emission features and silicate absorption in the mid infrared, (forbidden) atomic fine-structure lines in the mid and far infrared, and H_2 emission lines from warm molecular gas. Because of their strength (up to a few percent of the total infrared emission) and unique spectral signature, PAH features, which are ubiquitous in star-forming galaxies, present a means for measuring photometric redshifts with moderate resolution ($R \sim 8$) photometric bands. GEP will survey the sky with an imager comprised of 23 wavebands, with $R = 8$ from 10 to 95 μm and $R = 3.5$ from 95 to 400 μm (Fig. 1) – the bands are broader beyond 95 μm where the continuum is smoothly varying. The surveys will likely consist of four depths ranging from 3 square degrees to the entire sky, although the surveys are still being optimized and have not been precisely defined yet. Initial simulations indicate photometric redshift precision will range from $\sigma_z \sim 0.03$ to $\sigma_z \sim 0.1$; detailed simulations of redshift uncertainties remain to be done.

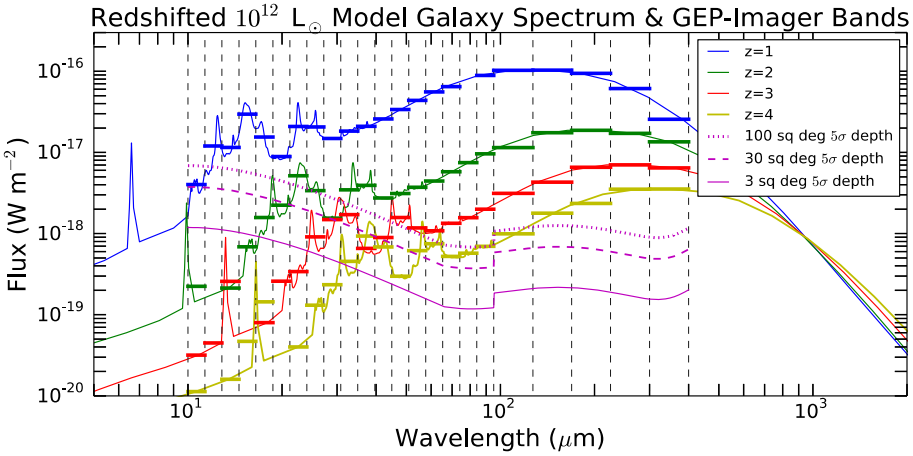

Figure 1. Model spectrum from Dale et al.[2] of a 10^{12} $L_\odot$ star-forming galaxy at redshifts $z = 1 - 4$ (10^{12} $L_\odot$ corresponds approximately to L^* at $z = 2$). Vertical dashed lines indicate the edges of the GEP-I photometric bands. The spectra display PAH emission features at mid-infrared wavelengths and thermal dust emission at longer mid-infrared through millimeter wavelengths. The colored horizontal bars within each band indicate the average emission in that band for the galaxy. The magenta lines indicate 5σ depths achievable with notional galaxy surveys assuming sensitivity limited by astrophysical sources (zodiacal light and Galactic dust emission). Atomic fine structure emission lines are not included in these models.

GEP will follow the imaging surveys with a comprehensive spectroscopic survey utilizing an R = 200, 24 – 193 μm spectrometer. With a range of ionization potentials of detectable far-infrared fine-structure lines, GEP will be able to measure spectroscopic redshifts, identify obscured AGN, and potentially measure the ionization parameters of the interstellar medium in galaxies (Table 1). The GEP will use approximately the first two years of its mission to do the photometric surveys with the imager. The deepest surveys will be done toward the ecliptic poles, where the zodiacal light is minimum. From the catalog of galaxies detected in those surveys, a subset spanning a range of luminosities, redshifts, PAH-to-continuum luminosity ratios and mid-infrared spectral slopes (indicating the relative contributions to luminosity by star formation and AGN) will be observed during the third and fourth years. This will generate a comprehensive catalog of star-forming galaxies in a broad range of luminosities, redshifts, and environments.

1.2 Basic Galaxy Evolution Probe Requirements and Concept

The science program necessitates some basic requirements for the GEP. First, wavelength coverage for the imaging survey must reach down to 10 μm to enable photometric redshifts with PAH features and reach to ~ 400 μm to encompass the peak of the spectral energy distribution of galaxies at redshifts $z \sim 3$. The spectrometer must cover low and high ionization potential lines from $z = 0$ to at least the peak of cosmic star formation. Second, the telescope must be cold – cooled cryogenically, not passively – so that the sensitivity is limited by astrophysical sources of emission and not the thermal emission of the telescope. Third, detector sensitivity should be sufficiently good that sources of astrophysical emission limit the sensitivity. Fig. 2 shows NEPs from astrophysical sources and the telescope emission; their combination is quadrature sets an upper limit for the detector NEPs. Fourth, for the deepest surveys, observations must be concentrated at the ecliptic poles where the zodiacal light is minimum. Fifth, the primary mirror must be as large a possible to minimize the affects of extragalactic confusion for measuring the peaks of galaxies' spectral energy distributions (confusion is expected to set in somewhere between 70 and 100 μm, detailed calculations are underway). Finally, the GEP Phase A – E cost must not exceed $1B (which limits the primary mirror size).

Table 1. Mid and far-infrared spectral lines that will fall within the GEP-S 24 – 193 μm spectral range at some redshifts.

SPECIES	REST WAVELENGTH (μm)	z = 2 WAVELENGTH (μm)	IONIZATION POTENTIAL (eV)	TRACES[a]	LUMINOSITY[b] RELATIVE TO L_{FIR} ($\times 10^{-4}$)
[S IV]	10.5	31.5	34.8	SF	…
PAH	11.25	33.75	N/A	SF	10
H_2 S(0)	12	36	N/A	H_2	…
[Ne II]	12.8	38.4	21.6	SF	3
[Ne V]	14.3	42.9	97.1	AGN	2
[Ne III]	15.6	46.8	41	SF/AGN	1
H_2 S(1)	17	51	N/A	H2	0.4
[S III]	18.7	56.1	23.3	SF	2
[Ne V]	24.3	72.9	97.1	AGN	2
[O IV]	25.9	77.7	54.9	AGN/SF	5
H_2 S(2)	28	84	N/A	H_2	…
[S III]	33.5	100.5	23.3	SF	3
[Si II]	34.8	104.4	8.2	SF	4
[O III]	51.8	155.4	35.1	SF/AGN	20
[O I]	63.2	189.6	N/A	SF	10
[O III]	88.4	> 193	35.1	SF	8
[N II]	122	> 193	14.5	SF	2
[O I]	145.5	> 193	N/A	SF	3
[C II]	158	> 193	11.3	SF	20

Table Notes: [a]SF denotes that the species predominantly traces star formation, AGN denotes that the species traces predominantly active galactic nuclei, and H_2 denotes direct tracers of the warm molecular gas, which is dominated by hydrogen. [b]Median line luminosities as a fraction of the total far-infrared luminosity are taken from Spinoglio, et al.,[3,4] Hemmati, et al.[5] ([C II]), and Fischer, et al.[6] The line luminosities should be taken as approximate.

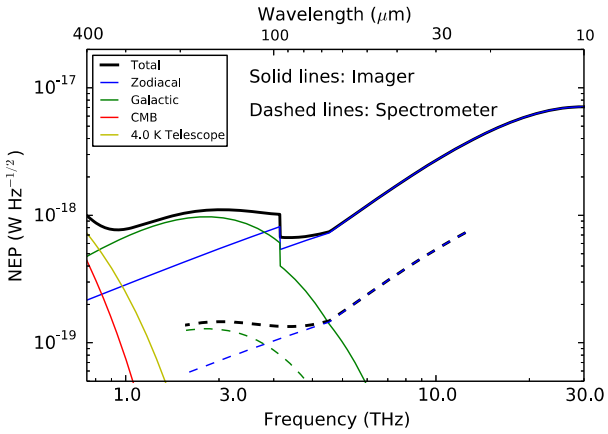

Figure 2. Limiting NEPs from various backgrounds, including zodiacal light, Galactic dust emission (from the Milky Way), the cosmic microwave background (CMB) radiation, and the telescope mirrors. KIDs must have NEPs below these values to contribute negligibly to the NEP. The GEP-I NEPs are discontinuous at 95 μm because the bandwidth changes. Assumptions include: emissivity of 1% for each telescope optic, 0.2 end-to-end optical efficiency, Galactic and zodiacal background emission for high ecliptic and Galactic latitudes ("Low Background" in http://ssc.spitzer.caltech.edu/warmmission/propkit/som/bg/),[7] and a CMB temperature of 2.726 K. Galactic dust emission is the astrophysical sensitivity limiter below 100 μm in wavelength and the zodiacal light is the sensitivity limiter above 100 μm. At 4 K, thermal emission from the telescope optics will not limit the sensitivity (although it would for $T \geq 6$ K at the long wavelengths).

The engineering concept design for the GEP is described in the remainder of this paper. The design was undertaken in late 2017 and early 2018, including four sessions with JPL Team-X for the science traceability matrix, both science payload instruments, and the mission. A CAD drawing of GEP is shown in Fig. 3. Section 2 describes the science payload, including the optical design and performance, kinetic inductance detectors (KIDs), the GEP imaging instrument (GEP-I), and the GEP spectrometer (GEP-S). Section 3 describes the mission implementation, including the galaxy survey strategy, the thermal design, and the bus. Both the thermal design and bus utilize components with space flight heritage. Section 4, the summary, reiterates important aspects of GEP reported in this paper.

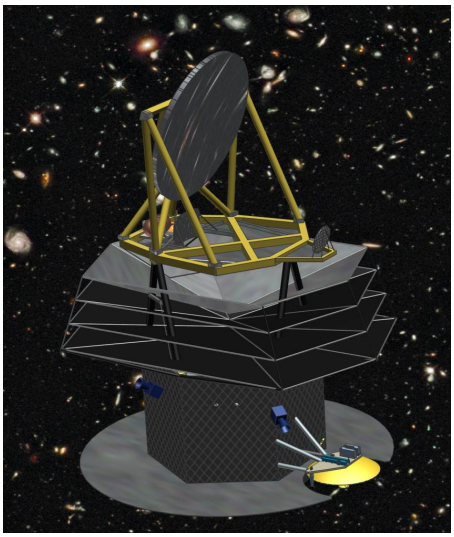

Figure 3. The Galaxy Evolution Probe. At any given time, the spacecraft will observe within ±20° of the great circle orthogonal to the Probe-Sun vector (which will always be within 15° of the Earth-Sun vector), keeping the solar panels pointed toward the Sun and the optics and instruments shielded from sunlight. The monolithic, off-axis primary mirror, with a 2.0 m diameter, is seen at the top, the instruments and cryogenics are below that, and the radiation shields prevent both solar and bus thermal radiation from reaching the cold telescope and science payload. The bus walls are radiators for head dissipation. The high-gain antenna is visible in the lower right. (Background image: Hubble Deep Field, credit NASA and STScI)

2. SCIENCE PAYLOAD

2.1 Optical design

The GEP optics includes an imager that provides input to a focal plane array (FPA) and four spectrometer entrance slits, and the spectrometers themselves. This section describes the common optical design up to the focus at the FPA or slits. Fig.4 shows the basic optical configuration.

The fundamental optical design requirement of the imager group common to all instruments is to collect light with the 2-meter diameter primary mirror and to form an f/9 focus at five interface planes (imager FPA, and the entrance slits to four different spectrometers). All five of these interface planes are fed by a common imaging telescope, an unobscured three-mirror anastigmat (TMA). The TMA is an often-used configuration that is well suited to the first order optical and mechanical requirements of this system (f/#, field of view, compact envelope, and accessible field stop and pupil stop). In addition to the three powered mirrors, the design includes a flat chopping mirror. The powered mirrors are all conic shapes (ellipsoid for the primary and tertiary, hyperboloid for the secondary). The parent surfaces are not coaxial, but have mutual tilts and decentrations to help reduce wavefront error.

The five interface planes are nearly co-planar, at the common focal surface of the TMA, with minor differences in final focus to minimize wavefront error in each channel. Thus, the angular field of view that the TMA must accommodate is driven not only by the required illuminated area of the imager FPA and the spectrometer slits, but also the mechanical size of each instrument (imager FPA and spectrometers) so that there is no mechanical interference between instruments. Based on the sizes of the FPA, slits and enclosures, the optimized field of view is 0.81°×0.88°. The centers of the spectrometer slits are in the plane of symmetry of the TMA so that they can be untilted with respect to the central ray to each spectrometer. The imager FPA is located out of plane.

The RMS wavefront error across the field of view of each instrument is diffraction limited at the minimum wavelength of 10 μm. Specific RMS wavefront error levels and geometric 100% encircled energy diameters for each instrument's field of view up to the TMA focus are listed in Table 2. Figure 5 shows a performance plot in terms of geometric spot diagrams across the range of the five instrument fields of view. The 100% encircled energy diameter is the equivalent of 1.45 arc seconds or less. However, to control cost and because of the lower limit of KID pixel sizes for a given readout bandwidth (see sections 2.2 and 2.3), the fabricated primary mirror will be required to be diffraction limited at 24 μm.

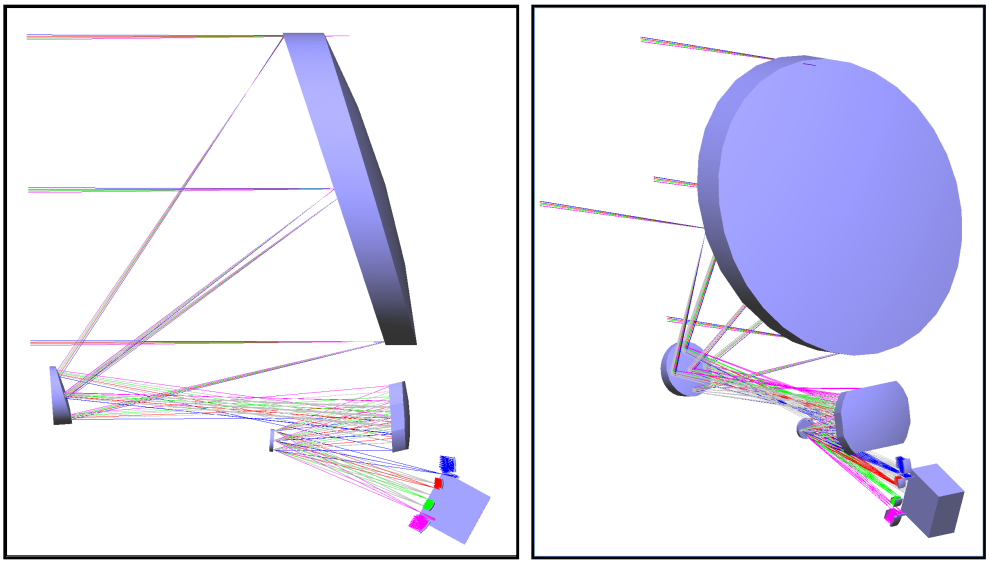

Figure 4. GEP optical configuration side view (left) and perspective view (right). Rays from infinity are shown striking the primary mirror from the left side of the figure and propagating through the optics. A field stop is located between the secondary and tertiary mirrors and the fourth optic is a chopping mirror located at an image of the primary mirror, forming a pupil stop. The large, blue box is the imager and the four smaller boxes (magenta, green, red, and blue) are the spectrometers.

Table 2. RMS wave-front error and geometric spot sizes across the imager and instrument fields of view.

INSTRUMENT INPUT	FAR FIELD ANGLE COVERAGE	RMS WFE MAXIMUM / AVERAGE (nm)	GEOMETRIC 100% ENCIRCLED ENERGY DIAMETER MAXIMUM / AVERAGE (arc seconds)
Imager FPA	x: -0.73° to -0.51° y: -0.72° to -0.21°	429 / 276	1.41 / 0.97
Slit to Spectrometer 1	x: -0.031° to +0.031° y: -0.615°	153 / 143	1.44 / 1.41
Slit to Spectrometer 2	x: -0.053° to +0.053° y: -0.355°	196 / 178	0.66 / 0.60
Slit to Spectrometer 3	x: -0.049° to +0.049° y: -0.930°	122 / 119	1.45 / 1.39
Slit to Spectrometer 4	x: -0.083° to +0.083° y: -0.050°	553 / 525	1.03 / 0.94

Stray light suppression is important in any long-wave infrared imaging system, and key elements for stray light reduction include a field stop (at the image of the far field) and a pupil stop (at the image of the primary mirror). The field stop prevents any out-of-field light from propagating beyond it, and thus eliminates the potential of light scattering off of structure and onto the FPA. The pupil stop, located at the chopping mirror, prevents the detectors from viewing structure outside the clear aperture of the mirrors that could be sources of light scatter. The TMA configuration naturally has both an accessible field stop and pupil stop.

The baseline for the GEP primary, secondary, and tertiary, and chopping mirrors is monolithic silicon carbide. However, a technology that shows promise for GEP and other Far-IR telescopes is silicon carbide mirrors with distributed figure control actuators[8]. In this technique, piezoelectric actuators are embedded into the backside of a lightweight silicon carbide mirror substrate. Through the application of DC voltage, these actuators can be used to locally warp the surface of the mirror and thus provide in-situ wavefront correction capabilities. This can be used to correct for a variety of optical errors in the telescope such as thermally induced figure distortions, gravitational sag of the primary mirror, and long-term material creep. There are also opportunities to significantly reduce the cost and complexity associated with mirror fabrication because the manufacturing tolerances can be relaxed as a result of the embedded figure control. Additional savings can be realized during telescope I&T as on-orbit performance specifications can be achieved under a variety of test conditions (i.e. room/cryogenic temperatures, zero/1g). A significant amount of work has been performed in this area for room-temperature, visible-wavelength applications and development activities are underway at JPL to extend these capabilities to cryogenic, far-infrared applications[9].

2.2 Kinetic inductance detectors and readout

KIDs will be utilized for GEP-I and GEP-S. KIDs are superconducting microresonators in which photons are detected by breaking Cooper pairs, resulting in surface impedance changes. KIDs as photon detectors were first described in Day et al.[10] Zmuidzinas[11] gave a comprehensive summary of KID physics and a review of architecture variations, sensitivities, and astronomical applications. Submillimeter NEPs sufficient for GEP-I have been demonstrated,[12] although continued sensitivity improvements must be obtained for GEP-S requirements.

Given that Si:As IBCs are a mature technology with arrays of 10^6 pixels adopted for JWST's MIRI,[13] why were KIDs selected for GEP's shortest wavebands? There are two reasons for this. First, Si:As IBCs have good sensitivity to wavelengths of 25 μm, diminishing sensitivity from 25 to 28 μm, and poor sensitivity beyond 28 μm. Thus, two types of detectors would have been required for GEP (with KIDs for wavelengths longer than 25 μm). Additionally, the MIRI Si:As IBCs have 15 μm pixels, which are incompatible with GEP's f/9 optics. While the engineering challenges of very different f/#s and operating temperatures (Si:As IBCs operate at 6 K) could be could be met, two instruments effectively would have been required *each* for GEP-I and GEP-S, which would have driven GEP above the cost cap. Second, Si:As

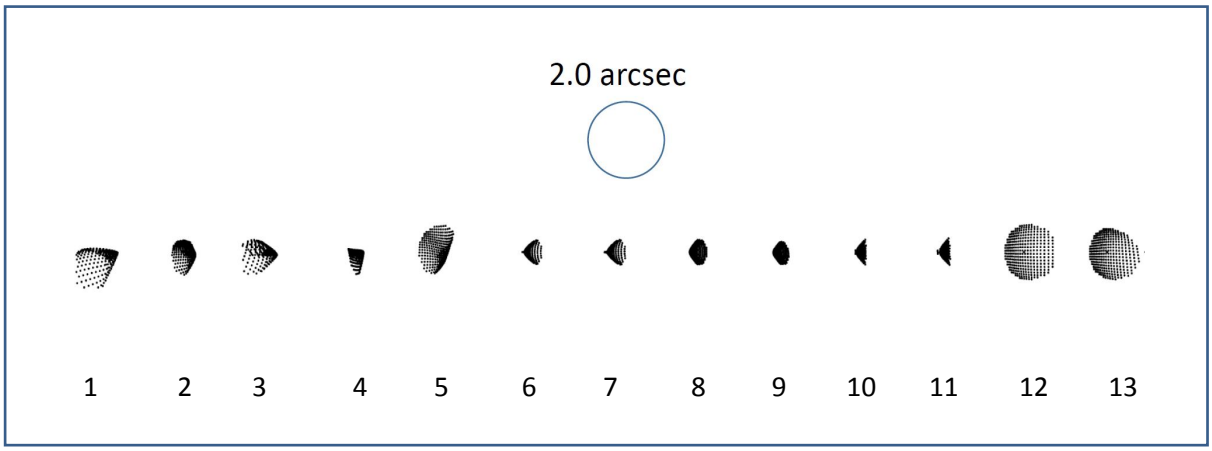

Figure 5. Geometric spot diagrams across imager and spectrometer input fields of view (far-field angles for the spots are listed in Table 3). The optical design provides diffraction-limited performance at 10 μm, meeting or exceeding the requirements for the GEP-I and GEP-S in all wavebands.

Table 3. Spot diagram field angles referring to Fig. 5.

FIELD NUMBER IN SPOT DIAGRAMS	FAR-FIELD ANGLES (°) (x, y)
1 – 5 (GEP-I)	(-0.735, -0.717), (-0.620, -0.463), (-0.735, -0.208), (-0.505, -0.717), (-0.505, -0.208)
6, 7 (GEP-S, Band 1)	(0.000, -0.615), (0.031, -0.615)
8, 9 (GEP-S, Band 2)	(0.000, -0.355), (0.053, -0.355)
10, 11 (GEP-S, Band 3)	(0.000, -0.930), (0.049, -0.930)
12, 13 (GEP-I, Band 4)	(0.000, -0.050), (0.083, -0.050)

IBC array fabrication has been halted. To fabricate arrays for GEP would necessitate restarting the development effort from a very low level. This was judged to meet or exceed the difficulty of achieving the required sensitivities and wavebands for GEP with KIDs, for which several development efforts are ongoing worldwide. Taken together, these reasons favor KIDs for GEP. Should KID efficiencies prove too low from 10 to 25 μm, Si:As IBCs could be adopted, although it would likely require a descope to remain under the cost cap.

Another viable detector technology for GEP is transition-edge sensors (TESs). They were not selected for GEP because of the additional complication that they bring to cryogenic focal plane architecture from integration with SQUID readouts. TES arrays have been used for astronomy from 53 μm[14] to millimeter wavelengths[15] and generally have higher TRLs (technological readiness levels). Similar to KIDs, TES architectures would have to be modified for operation down to 10 μm. This should be possible; thus, TESs serve as another alternative detector technology for GEP. At the time of preparation for a GEP Phase A study, a trade study will determine which detector technology is most mature and would be easiest to integrate with the spacecraft. For the time being, the baseline is KIDs for the reasons described.

Back-illuminated, lumped-element, microlens-coupled aluminum KIDs will be used for GEP-I (with 25,735 total detectors) and GEP-S (with 24,640 total detectors). They require a 100 mK bath temperature. For wavelengths greater than ~ 100 μm, the detector architecture in the left panel of Fig. 6 will be adopted. Aluminum makes a good resonator choice because its long quasiparticles lifetimes and high electrical conductivity enable small active area (absorber) volumes, which translates to high sensitivity. Down to approximately 100 μm in wavelength, efficient absorbers can be achieved with thin lines spaced closely enough that the meander 'grid' approximates and absorbing sheet well.

However, below ~ 100 μm the lines would have to be so close together and so thin that they would be difficult to fabricate with a simple unidirectional meander as shown in the left panel of Fig. 6. Thus, the architecture must be modified to create higher resistivity and therefore greater photon absorption efficiency. The concept in the right panel of Fig. 6 achieves this. The vertical lines (separated by 2 μm) sense the vertical electric field polarization. Their width is 100 nm, which can be written by e-beam lithography. The meanders extending horizontally provide additional (resistive) electrical path length and thereby enable high absorption efficiency. Distributed capacitance is added via the additional meander to offset the distributed inductance of the lengthier absorber meander. The unit cell pattern is repeated to cover the entire absorber area. Initial electromagnetic simulations indicate high absorber efficiency, although devices will have to be fabricated and tested before this architecture will be adopted.

GEP-I and GEP-S will share the same set of readout electronics since the imager and spectrometer have separate observing modes. After checkout on orbit, observations will be done with the imager for ~2 years, then microwave switches will feed the spectrometer KIDs signals to the electronics instead of the imager KID signals. There will be 23 readout channels corresponding to the number of GEP-I wavebands and detector modules; the four GEP-S spectrometers will have their readouts distributed over these 23 modules. The total estimated power consumption is approximately 600 W.

For the GEP KIDs, the cryogenic focal plane array is fully passive: the only active components are low-noise amplifiers at 4 K and 20 K, the resonators and all elements of the focal plane are passive. The readout electronics are on the warm side of the spacecraft, they are similar to those baselined for the Origins Space Telescope (OST), and they are being studied as part of a broader far-IR detector technology development plan that is being prepared for a report to the Astro2020 Astronomy Decadal Survey. Laboratory, ground-based, and balloon-borne readout systems exist based on field-programmable gate array (FPGA) technology;[16] the primary concern for moving to high-pixel-count flight instruments is power dissipation. Fortunately, this problem benefits from the rapid advancement of integrated analog and digital electronics driven by telecommunications needs.

The basic approach is to divide the detector arrays into circuits, each of which processes some number N_{Res} of detectors. N_{Res} will be on order 1,000–2,000, depending on the choice of frequency range and frequency spacing. The frequency range results from a trade between enabling sufficiently small pixels (resonator area scales as $1/f^2$, where f is frequency), and minimizing power dissipation on the warm side, which scales as f. Evaluating this trade in a conservative manner for GEP, resonant frequencies were baselined between 650 and 1650 MHz: this 1.3-octave range accommodates N_{Res} = 1,500 detectors log spaced at approximately 1 part in 1,700 based on quality factors obtained in our typical laboratory and ground-based systems.[17] The frequency choice enables an area-averaged pixel area of 0.09 square millimeters, a good match to the GEP imager and spectrometer designs.

In each circuit, a waveform consisting of N_{Res} pure radio-frequency (RF) tones is generated. The waveform propagates on coaxial line through the thermal stages to the focal plane array, where each tone interacts with its individual resonator. The return signal on a separate line carries the same waveform, but with each tone having a phase shift encoding resonance frequency of its corresponding resonator. The electronics must digitize and store the returning waveform at a base sampling rate set by the total bandwidth of the system (~1 – 2 GSPS), then Fourier transform to frequency space and extract the I and Q (in-phase and quadrature) components of all tones relative to the input signal at the science sampling rate (~1 kHz). The total power dissipation scales as the maximum baseband frequency equal to the total frequency range if mixing up; this is 1 GHz for GEP. Both the analog-to-digital conversion (ADC) and digital signal processing, as well as their interfacing, can be power intensive depending on the implementation. The existing FPGA-based readout, which has had no optimization for power consumption, processes a single circuit with frequencies up to 500 MHz and requires about 50 W.

However, massive gains are now becoming available. An example is the new Xilinx RF system-on-chip (SoC) that integrates the ADC with FPGA-like programmable digital signal processing logic in a single chip based on 16 nm gate CMOS transistors. A single chip provides eight channels, each capable of processing 2 GHz at 12 bits depth. With the associated waveform generation capability, it represents approximately 8 x (2 / 0.5) = 32 times the processing capability of the existing FPGA-based readout. A board with this chip is being released by Abaco Systems as of this writing. Initial power dissipation estimates are 50 W for this board at full utilization.

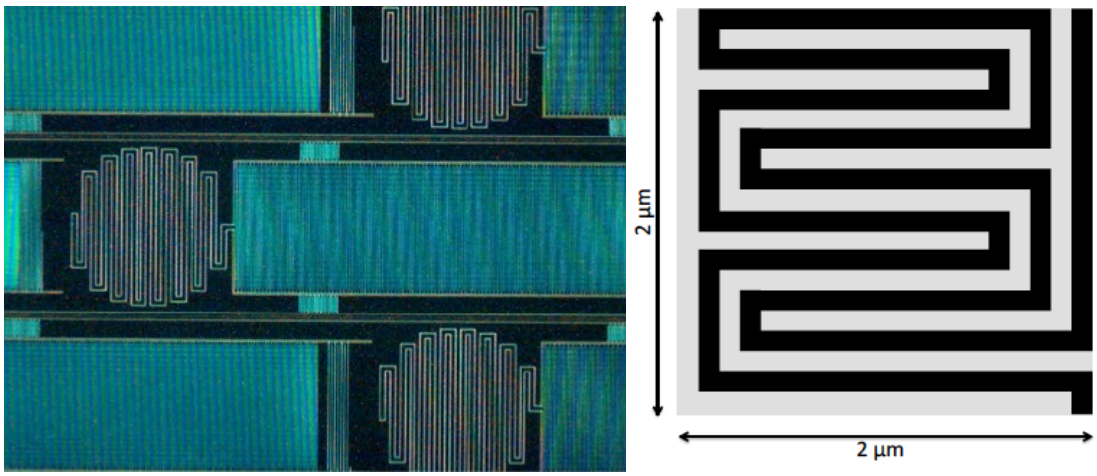

Figure 6. (Left) Lumped-element KIDs will be used for the longer GEP-I and GEP-S wavebands – likely greater than λ ~ 100 µm. A photograph (from Glenn, et al.[20]) of a LEKID is shown on the left: the (lens-coupled, back-illuminated) absorbers are the inductors formed by the meanders with circular envelopes and the interdigitated capacitors are the rectangular structures. The pixel pitch (absorber centroid to absorber centroid) is 400 µm. (Right) A unit cell of the absorber of a KID concept for 10 µm wavelength: the conductor is black with bare dielectric substrate shown as grey. The absorber absorbs radiation with a vertical polarization in the drawing.

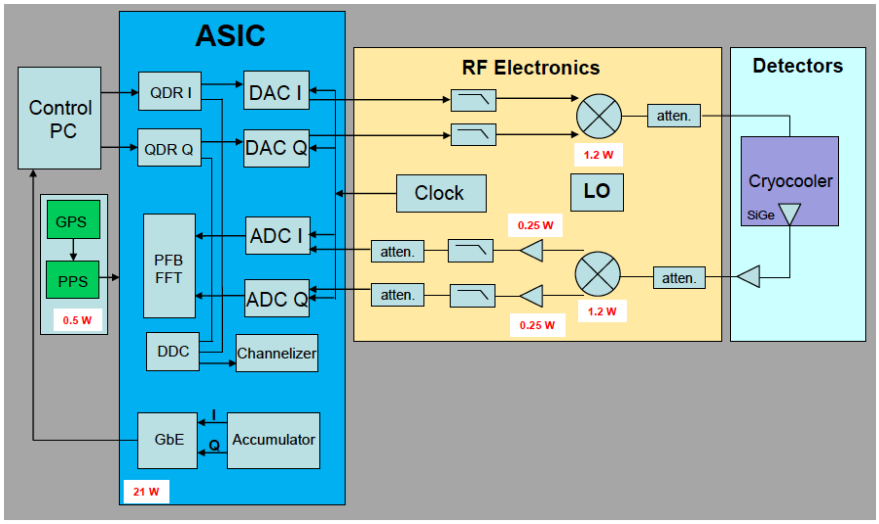

Figure 7. Signal chain for the GEP KIDs. All electronics are room temperature except the amplifiers at 4 K and 20 K (and the KIDs themselves at 0.1 K). The power consumptions are per module – there will be 23 modules.

While neither of the existing systems is flight-qualified, mixed-signal application-specific integrated circuits (ASICs) that integrate ADCs and signal processing have been developed for similar applications.[18,19] These systems typically have lower power dissipation than their programmable-logic counterparts, so we consider the power performance of the new Xilinx / Abaco Systems system as a reasonable estimate of what can be obtained on the GEP timescales with an ASIC that is developed in the same 16 nm fabric. Nevertheless, for the GEP concept study, we adopted a much more conservative assumption based on worst-case scalings of as-built ASICs, which are typically 3-5 bits, to our larger bit depth. These systems are in 65 nm gate fabric, so they are naturally much more power-intensive than the new smaller-gate technology. The approach is captured in Figure 7. The study baseline is that each 1 GHz circuit will require 25 W, including the RF up and down conversion, but we fully expect that even lower dissipation can be obtained as GEP moves closer to implementation, whether it is via a custom ASIC or via development of a commercial flight-worthy system similar to the RF SoC.

2.3 GEP-I: Imager

The GEP-I concept is designed to obtain multiple measurements of every galaxy that is observed in each of the 23 wavebands by repeatedly scanning areas of sky. The instrument is fed an f/9 beam from the telescope and reimaging optics, with a cold stop at 4 K where the chopping mirror (which is used for modulation during GEP-S observations) resides. Each of the wavebands occupies the same amount of focal plane area, 0.002 square degrees, half of which is occupied by detectors and half of which is allotted for filter mounting. The shortest wavebands are in the center (where the optical performance is the best) and the longest wavebands are at the two edges (Fig. 8.) Metal-mesh filters define the bandpasses, which are listed in Table 4. Bands 1 – 18 are spectral resolution R = 8, whereas bands 19 – 23 are spectral resolution R = 3.5.

GEP's optical performance is diffraction limited at 10 μm. However, for fabrication and construction, the primary mirror is specified to be diffraction limited at 24 μm, which corresponds approximately to a 3 arcsecond beam size (FWHM). A main reason for this is that the smallest KID pixels size we expect to be able to fabricate without exceeding the readout bandwidth is 300 μm, which corresponds to 3.43 arc seconds. Thus, bands 1 – 13 will not be Nyquist sampled (bands 14 – 23 will be). Should greater bandwidth become feasible through improvements in data acquisition and computing speed, the pixel sizes could be reduced, recovering Nyquist sampling at shorter wavelengths.

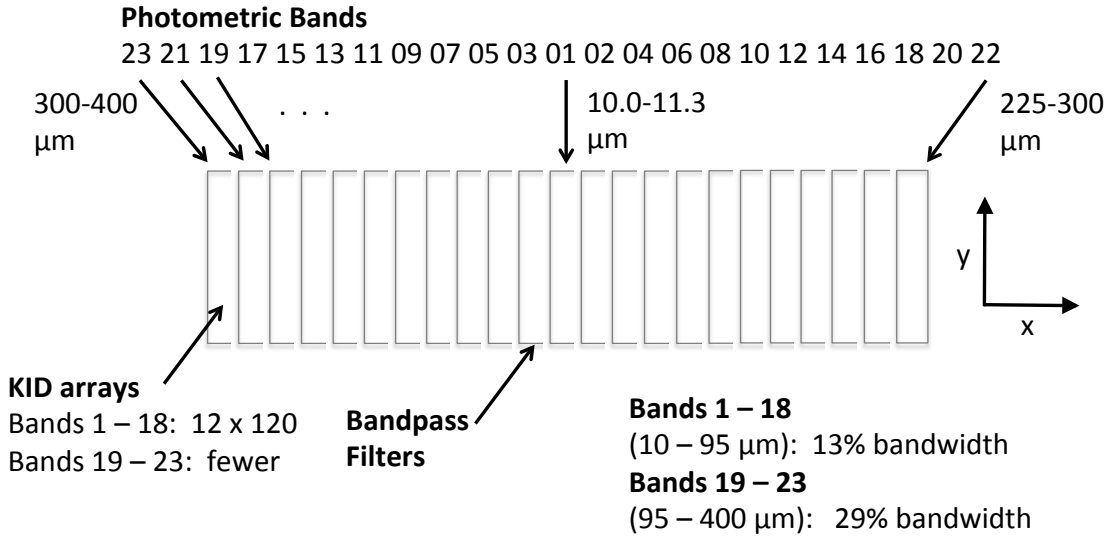

Figure 8. Imager (GEP-I) focal plane layout concept. The 50% active area allows for bandpass filter mounts. Bands 1 (10.0 – 11.3 μm) through 15 (57.7 – 65.4 μm) have 1,440 KIDs (arrays of 12 horizontally in the diagram by 120 vertically), with 3.43 arcsecond pixels (300 μm square). The longer-wavelength bands have fewer, larger KIDs such that the focal plane area occupied by each photometric band is approximately the same. For example, Band 23 (300 – 400 μm) has 46 KIDs 1,560 μm square.

Table 4. GEP-I wavebands.

WAVEBAND	1	2	3	4	5	6	7	8	9	10	11	12
CENTRAL WAVELENGTH (μm)	10.7	12.1	13.7	15.5	17.6	19.9	22.6	25.6	29.0	32.9	37.3	42.3
WAVEBAND	13	14	15	16	17	18	19	20	21	22	23	…
CENTRAL WAVELENGTH (μm)	47.9	54.3	61.5	69.7	79.0	89.6	111	148	197	263	350	…

2.4 GEP-S: Spectrometer

GEP's science requirements call for observing mid and far-infrared atomic fine-structure lines from galaxies over a range of redshifts. Specifically, the 24.3 μm [Ne V] line starting at $z = 0$ (for AGN identification) and the 63.2 μm [O I] line at $z = 2$. The entire bandwidth should be available to identify spectral lines for galaxies of unknown redshift. Sufficient spectral resolution is required to achieve good sensitivity (through dispersion of the astrophysical background photons). Spectral resolution R = 200 meets these requirements.

GEP-S is implemented with four spectrometers, identified as Band 1 (24 – 42 μm), Band 2 (40 – 70 μm), Band 3 (66 – 116 μm), and Band 4 (110 – 193 μm). Each Band, or spectrometer module, is comprised of an enclosure, a slit, a collimator, a diffraction grating (operated in first order), a focusing mirror, and an array of KIDs. Bands 1 and 2 each have 7,840 KIDs and Bands 3 and 4 each have 4,480 KIDs. The slit lengths for Bands 1 – 4 are 3.8, 6.4, 6.0 and 10.0 arc minutes, respectively, enabling spectral mapping of nearby galaxies and 'blind' spectral surveys for galaxies identified via their line emission. Fig. 9 shows the optical configurations for Bands 2 and 4. As with the imager, the shortest-wavelength Bands (1 and 2) are placed nearest to the center of the field of view, where the optical performance is the best (Fig. 4).

3. MISSION IMPLEMENTATION

The baseline GEP flight system is designed as a Class B mission with significant science and engineering margins utilizing a combination of high heritage designs and newly available components, resulting in a low risk mission below the Probe class cost cap. The flight system utilizes the Ball Aerospace BCP2000 bus, of Kepler heritage, which is customized to meet the science and mission requirements of GEP. The four-year mission is divided into an imaging and spectroscopy campaign where a total of 250 TB of observational data will be downlinked. Table 5 summarizes high-level GEP mission parameters.

3.1 Mission design and observing modes

The GEP mission schedule has a launch onboard a Falcon 9 on January 1, 2029 and transit to an Earth-Sun L2 halo orbit with a maximum Sun-Earth-Probe angle of 15°. The transit to L2 will require 150 m/s ΔV, while orbit maintenance for the four-year mission requires 10 m/s ΔV over 16 maneuvers. During transit, GEP will begin cooling down the payload so that observations can begin at L2 arrival.

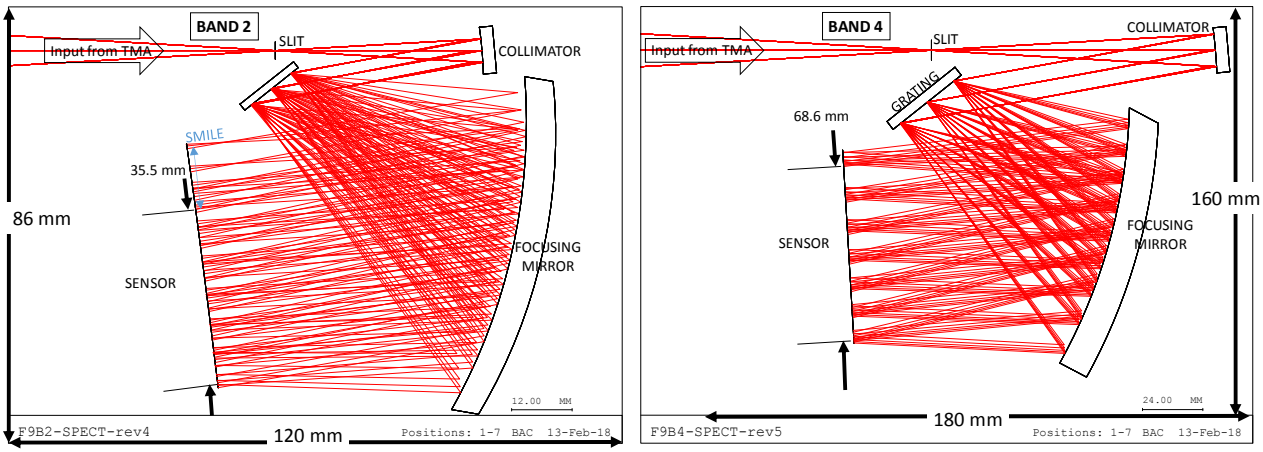

Figure 9. GEP-S spectrometer optical configurations for Band 2 (40 – 70 μm; left) and Band 4 (110 – 193 μm; right). All four spectrometer modules are fed by f/9 beams and produce a spectral resolution of $R = 200$. All optics except filters are reflecting.

The deep scan strategy entails rotating the telescope bore sight about a vector pointed near or along the Sun-Probe axis, with the north and south ecliptic pole fields accessible at all times throughout the mission. The all-sky survey is performed during downlink, where the bore sight rotates about the Earth-Probe axis owing to the static high gain antenna

Table 5. GEP mission parameters. The GEP mission will provide 250 TB worth of insights into galaxy evolution and star formation rates using a high heritage, Ball Aerospace bus.

MISSION PARAMETER	SPECIFICATION
Destination	Sun-Earth L2, Maximum 15° Sun-Earth-Probe angle
Launch Date	January 1, 2029
Mission Duration	4 years
Mission Class	B, dual string (hot/cold redundancy)
Bus Heritage	Ball BCP2000 (e.g. Kepler)
Mass (CBE[a] + Contingency)	1520 kg
Max Power (CBE + Contingency)	3260 W
Stabilization	Three axis (0.5 arc seconds per 3 minutes), non spinning
Telescope Temperature	4 K
Focal Plane Temperature	0.1 K
Field of Regard	> ±20°
Total Mission Science Data	> 250 TB

Table notes: [a]CBE denotes current best estimate.

pointing requirement. As the passive thermal shield allows for a field of regard of over ±20°. There is over 5° margin in pointing away from the Earth

As the imager and spectrometer use the same readout electronics, only one instrument will observe at a time. Both the imager and spectrometer share a scan survey observing mode, where differential detection is performed as the spacecraft slews at approximately 60 arc seconds / second. This mode is used in GEP-I's deep surveys of the ecliptic poles and broad all-sky survey and GEP-S's blind survey mode. GEP-S will also have a pointed observation mode in which a chopping mirror, with a total throw of ± 0.2°, modulates the signal for *1/f* noise mitigation and for background subtraction.

3.2 Thermal design

The thermal system for GEP employs multiple passive and active stages, shown in Fig. 10, to meet the temperature intercepts required for science operations (details of the thermal design are presented in Moore et al.[21]). In this system, a continuous multi-stage adiabatic demagnetization refrigerator (ADR) provides cooling for the detectors at 100 mK with a 1K thermal intercept to reduce thermal noise and parasitic loads. Goddard Space Flight Center has extensive experience producing flight ADRs and the proposed system utilizes high heritage subcomponents from previous missions. A hybrid Joule-Thomson and Stirling cryocooler intercepts heat at 4 K from the ADR, cryogenic amplifiers, and parasitic loads. The hybrid cooler also has a 20 K intercept to cool a second stage of amplifiers for the detector signals, and an active thermal shield to reduce radiant loads from the V-groove system. The V-groove radiators are passively cooled shields that intercept conducted loads from the bipods and harnesses and radiative loads from the Sun. With non-deployable V-grooves (that fit to the dynamic envelope of a Falcon 9 fairing), the spacecraft can tilt ±21°, maintaining all cryogenic components in the shadow cone and thus preserving thermal system operability. The cooler and ADR electronics dissipate heat at room temperature (~300 K) in the spacecraft bus. The system is composed of reliable, high flight heritage subcomponents, which can be implemented with low risk to the science objectives.

3.3 Bus: power, propulsion, attitude control, command and data handling, and telecommunications

To reduce risk and cost, the GEP spacecraft concept design has no deployables. The only mechanism is the chopping mirror mechanism in the science payload.

The driving power mode used to size the power subsystem is simultaneous downlink and observation, using 3.15 kW, which assumes 90% system contingency. An 88 Amp-hour secondary, lithium-ion battery is sized for 3 hr launch and

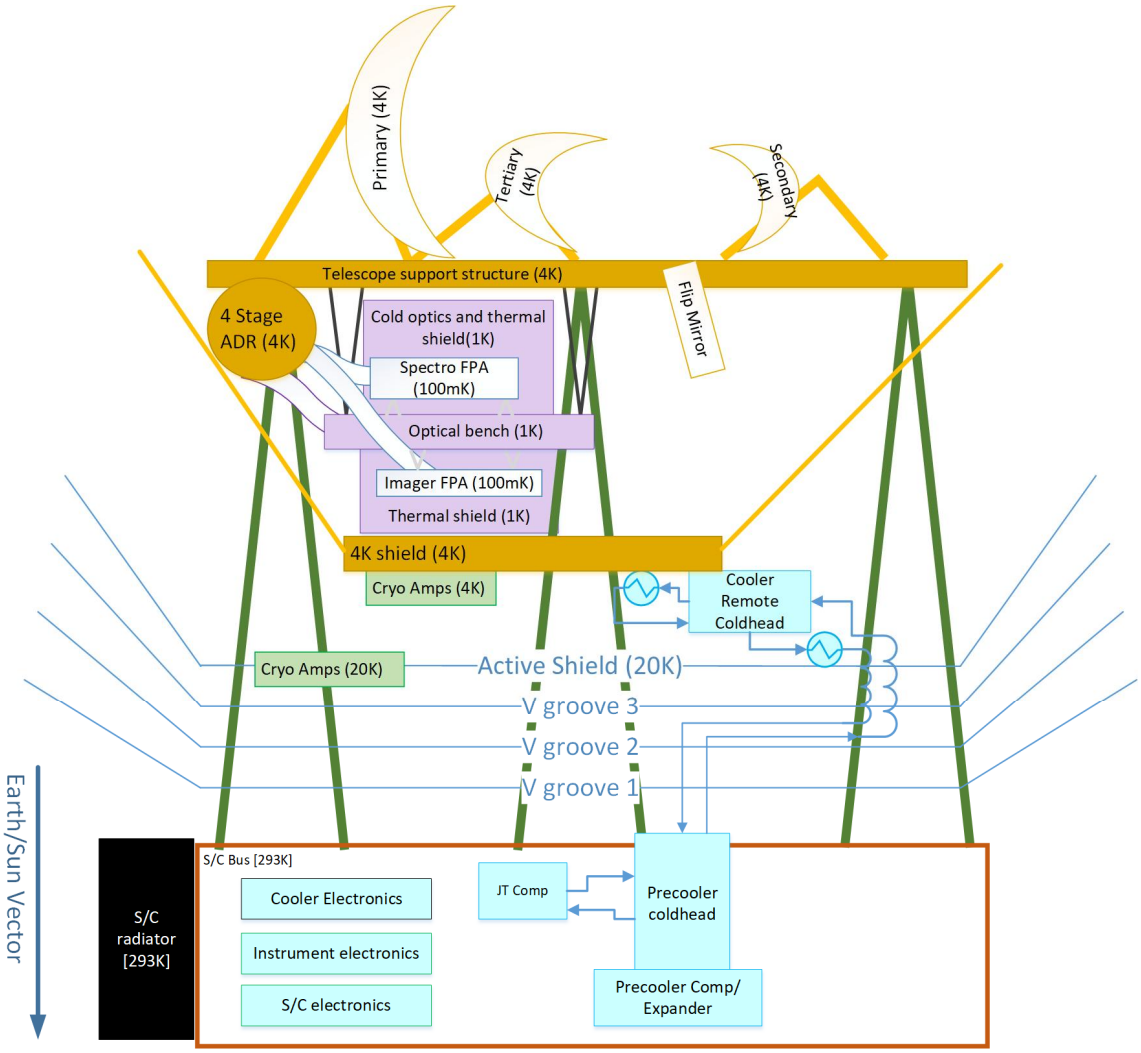

Figure 10. GEP thermal block diagram. The electronics and cooler reside in the warm (approximately room temperature) bus, while the telescope optics and first stage of detectors signal amplification reside at 4 K, the optics bench is 1 K, and the detectors are 100 mK. There is a second stage of amplification at 20 K. An active radiation shield and three passive V-groove shields separate the bus and cryogenic stages and prevent solar radiation from reaching the cold stages.

checkout, with 65% depth of discharge. To maintain the payload at cryogenic temperatures, the GEP spacecraft must assure nominal operating conditions for the bus components. Heat from payload electronics and JT cooler is radiated by 10.5 m^2 of radiators mounted on the bus behind the solar panels.

To meet GEP's modest propulsive requirements, a simple monopropellant hydrazine blowdown system is used. A single 22 N main thruster will provide thrust for halo orbit insertion, while four 4 lbf thrusters are used to desaturate GEP's reaction wheels once per day.

GEP's ACS subsystem is sized to meet the pointing stability requirement of GEP-S's pointed observing mode, requiring 0.5 arc second (1σ) stability for 300 s and 0.5 arc second pointing knowledge. In the design, the required pointing knowledge is provided by three low-cost, high-accuracy Ball CT2020 star trackers, with a fourth carried for redundancy. Star tracker telemetry is used to update a SIRU generating high refresh rate pointing knowledge stored in observational metadata. Three Sun sensors will be flown to provide redundant pointing knowledge during safe mode. Three-axis stabi-

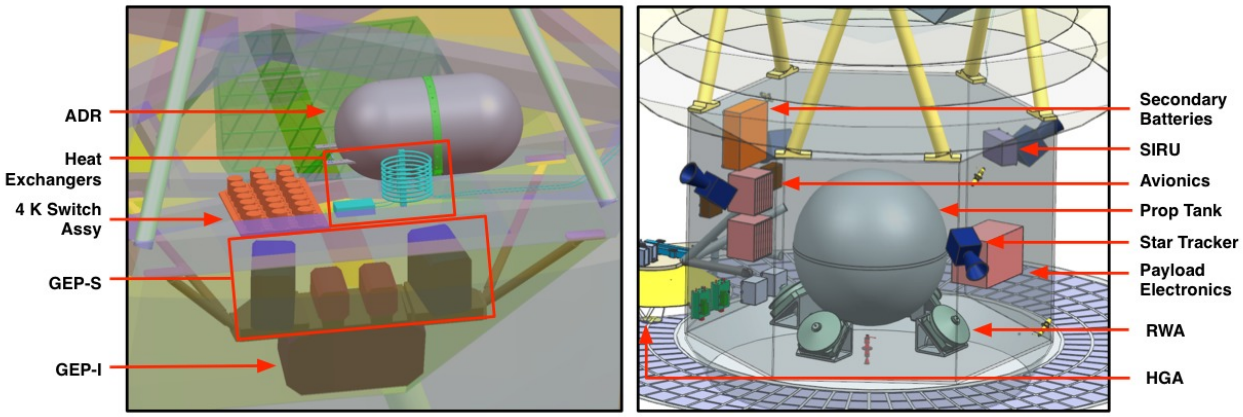

Figure 11. Configuration of the GEP scientific payload and bus. (Left) GEP-I and GEP-S instrument boxes and elements of the cryogenic system. The 4 K switch assembly is a bank of GHz switches that route either the GEP-I or GEP-S detector signals to the readout electronics (GEP-I and GEP-S do not observe simultaneously). (Right) GEP bus with primary components labeled. The solar panel skirt is visible at the bottom and the science payload resides above the structure shown in the panel.

lization for the bus and payload is provided by four Honeywell 25 reaction wheels, requiring one daily desaturation sized for the imager survey mission assuming a 30% momentum storage margin.

Two RAD750 flight computers will be flown in a dual-string configuration. Four storage cards provide a total of over 760 GB of available storage, three times the data volume to be generated daily.

GEP follows in the footsteps of JWST and other missions taking advantage of the DSN's evolving Ka-band capabilities. GEP uses redundant dual polarization Ka-band downlink for science data and S-band for command and telemetry. A 0.65 m static high gain antenna (HGA) is baselined to reduce cost and vibration and enables 260 Mbps science data downlink with 7.9 dB to the DSN's 34 m BWG ground stations. Two low-gain S-band antennas offer 4π steradian coverage for persistent access. Fig. 11 shows the GEP payload and bus configuration.

4. SUMMARY

There currently exists no medium-scale NASA Astrophysics observatory class – a Probe class – that allows for more ambitious science than SMEXs and MIDEXs and for a faster launch cadence that Surveyor class mission. The Galaxy Evolution Probe is a concept for a space observatory that would enable vast surveys of star formation in galaxies encompassing the bulk of the cosmic history of star formation. Utilizing a 23 band imager, GEP will simultaneously identify star-forming galaxies and measure their redshifts photometrically from emission features of PAH molecules. By measuring emission from small and large dust grains, warm molecular gas, and ionized atomic gas, GEP will be able to simultaneously measure the star formation and AGN accretion rates in galaxies from the local Universe to before the star-formation peak at $z \sim 2$, assessing the causes of the precipitous decline in star formation for the first time. Both the GEP-I and GEP-S will utilize KIDs, which require 100 mK operating temperature. Further investment in KID technology is necessary to improve sensitivities to that required for GEP-S and to extend wavelength coverage down to 10 μm. A technology development plan is being authored to guide the development. GEP requires a 2.0 m telescope to limit astrophysical confusion and to enable it reach to the peak in cosmic star formation density for moderate-luminosity galaxies (L*), which can be realized under the $1B Probe cost cap. To enable the GEP to be background limited – the ultimate sensitivity that can be achieved – the telescope optics will be actively cooled to 4 K. The optical system has been designed and is diffraction limited, the thermal system (which utilizes no consumables) is designed, and the spacecraft bus utilizes components with substantial space-flight heritage. With instrument and mission concept studies complete, the GEP schedule has a start in late 2023, a launch date of early 2029, and a prime science-mission duration of 4 years.

ACKNOWLEDGEMENTS

The authors gratefully acknowledge NASA award number NNX17AJ89G in support of this work. The authors also gratefully acknowledge discussions with Phil Appleton, Steve Eales, Matt Griffin, GSFC (regarding the ADR), Bill Purcell, and important early work by Anita Sengupta. The research described in this paper was partially carried out at the Jet Propulsion Laboratory, a part of the California Institute of Technology, under a contract with the National Aeronautics and Space Administration.

REFERENCES

[1] Madau, P., and Dickenson, M., "Cosmic Star-Formation History," Annual Review of Astronomy and Astrophysics, 52, 415-486 (2014).
[2] Dale, D.A., Helou, G., Magdis, G.E., Armus, L., Díaz-Santos, T., and Shi, Y., "A Two-Parameter Model for the Infrared/Submillimeter/Radio Spectral Energy Distributions of Galaxies and Active Galactic Nuclei," Astrophysical Journal, 784, 83-93 (2014).
[3] Spinoglio, L., Dasyra, K.M., Franceschini, A., Gruppioni, C., Valiante, E., and Isaak, K., "Far-IR/Submillimeter Spectroscopic Cosmological Surveys: Predictions of Infrared Line Luminosity Functions for z < 4 Galaxies", Astrophysical Journal, 745 (2), 171-190 (2012).
[4] Spinoglio, L., Dasyra, K.M., Franceschini, A., Gruppioni, C., Valiante, E., and Isaak, K., "Erratum: Far-IR/Submillimeter Spectroscopic Cosmological Surveys: Predictions of Infrared Line Luminosity Functions for z < 4 Galaxies", Astrophysical Journal, 791 (2), 138-147 (2014).
[5] Hemmati, S., Yan, L., Díaz-Santos, T., Armus, L., Capak, P., Faisst, A., and Masters, D., "The Local [C II] 158 μm Emission Line Luminosity Function", Astrophysical Journal, 834 (1), 36-45 (2016).
[6] Fischer, J., Abel, N.P., González-Alfonso, E., Dudley, C.C., Satyapal, S., van Hoof, P.A.M., "A Far-Infrared Spectral Sequence of Galaxies: Trends and Models," Astrophysical Journal, 795, 117-140 (2014).
[7] "Spitzer: Background Estimates in Sensitivity Plots," http://ssc.spitzer.caltech.edu/warmmission/propkit/som/bg/ (28 February 2018).
[8] Hickey, G., Barbee, T., Ealey, M., and Redding, D., "Actuated hybrid mirrors for space telescopes," Space Telescopes and Instrumentation 2010: Optical, Infrared, and Millimeter Wave, International Society for Optics and Photonics, 7731, p. 773120 (2010).
[9] Steeves, J., Wallace, J.K., Redding, D., Lawrence, C., Gaier, T., and Bartman, R., "Active mirrors for future space telescopes", Advances in Optical and Mechanical Technologies for Telescopes and Instrumentation, International Society for Optics and Photonics 10706-38 (2018).
[10] Day, P.K., LeDuc, H.G., Mazin, B.A., Vayonakis, A., and Zmuidzinas, J., "A broadband superconducting detector suitable for use in large arrays," Nature, 425, 817-821 (2003).
[11] Zmuidzinas, J., "Superconducting Microresonators: Physics and Applications," Annual Review of Condensed Matter Physics, 3, 169-214 (2012).
[12] Janssen, R.M.J., Baselmans, J.J.A., Endo, A., Ferrari, L., Yates, S.J.C., Baryshev, A.M., and Klapwijk, T.M. "Performance of Hybrid NbTiN-Al Microwave Kinetic Inductance Detectors as Direct Detectors for Submillimeter Astronomy," Proceedings of the SPIE, 9153, 7pp. (2014).
[13] Ressler, M.E., Sukhatme, K.G., Franklin, B.R., Mahoney, J.C., Thelen, M.P., Bouchet, P., Colbert, J.W., Cracraft, M., Dicken, D., Gaustad, R., Goodson, G.B., Eccleston, P., Moreau, V., Rieke, G.H., and Schneider, A., "The Mid-Infrared Instrument for the James Webb Space Telescope, VIII: The MIRI Focal Plane System," Publications of the Astronomical Society of the Pacific, 127, 675-685 (2015).
[14] Staguhn, J.G., Benford, D.J., Dowell, C.D., Fixsen, D.J., Hilton, G.C., Irwin, K.D., Jhabvala, C.A., Maher, S.F., Miller, T.M., Moseley, S.H., Sharp, E.H., Runyan, M.C., and Wollack, E.J., "Performance of Backshort-Under-Grid Kilopixel TES Arrays for HAWC+," Journal of Low Temperature Physics, 184, 811-815 (2016).
[15] Staguhn, J., Allen, C., Benford, D., Sharp, E., Ames, T., Arendt, R., Chuss, D., Dwek, E., Kovacs, A., Maher, S., Marx, C., Miller, T., Moseley, S.H., Navarro, S., Sievers, A., Voellmer, G., and Wollack, E., "GISMO, a 2 mm Bolometer Camera Optimized for the Study of High Redshift Galaxies", Journal of Low Temperature Physics, 151, 709-714 (2008).

[16] Gordon, S., Dober, B., Sinclair, A., Rowe, S., Bryan, S., Mauskopf, P., Austermann, J., Devlin, M., Dicker, S., Gao, J., Hilton, G.C., Hubmayr, J., Jones, G., Klein, J., Lourie, N.P., McKenney, C., Nati, F., Soler, J.D., Strader, M., and Vissers, M., "An Open Source, FGPG-Based LeKID Readout for BLAST-TNG: Pre-Flight Results", Journal of Astronomical Instrumentation, 05, 1641003, 13 pp. (2016).
[17] Swenson, L.J., Day, P.K., Dowell, C.D., Eom, B.H., Hollister, M.I., Jarnot, R., Kovács, A., Leduc, H.G., McKenney, C.M., Monroe, R., Mroczkowski, T., Nguyen, H.T., and Zmuidzinas, J., "MAKO: a pathfinder instrument for on-sky demonstration of low-cost 350 micron imaging arrays", Proc. SPIE, 84520P, doi: 10.1117/12.926223, 10 pp. (2012).
[18] Hsiao, F., Tang, A., Kim, Y., Drouin, B., Chattopadhyay, G., and Chang, M.-C.F, "A 2.2 GS/s 188mW spectrometer processor in 65nm CMOS for supporting low-power THz planetary missions," IEEE Custom Integrated Circuits Conference, DOI: 10.1109/CICC.2015.7338367 (2015).
[19] Zhang, Y., Kim, Y., Tang, A., Kawamura, J., Reck, T., and Chang, M.-C.F., "A 2.6GS/s Spectrometer System in 65nm CMOS for Spaceborne Telescope Sensing," IEEE International Symposium on Circuits and Systems (ISCAS), DOI: 10.1109/ISCAS.2018.8351690 (2018).
[20] Glenn, J., Fyhrie, A., Wheeler, J., Day, P.K., Eom, B.-H., and Leduc, H.G., "Low-volume aluminum and aluminum / titanium nitride bilayer lumped-element kinetic inductance detectors for far-infrared astronomy", Proc. SPIE, 99140Z (2016).
[21] Moore, B., Lasco, J., Bradford, C.M., Amini, R., Larson, M., Jahromi, A., Glaister, D., and Glenn, J., "Thermal architecture of the Galaxy Evolution Probe", paper 10698-181 these proceedings.